BIOCHEMISTRY
including biophysical chemistry & molecular biology

Article

pubs.acs.org/biochemistry

Role of Thr218 in the Light-Driven Anion Pump Halorhodopsin from *Natronomonas pharaonis*

Kousuke Shibasaki, Hiroaki Shigemura, Takashi Kikukawa, Masakatsu Kamiya, Tomoyasu Aizawa, Keiichi Kawano, Naoki Kamo, and Makoto Demura*

Faculty of Advanced Life Science, Hokkaido University, Sapporo 060-0810, Japan

Supporting Information

ABSTRACT: Halorhodopsin (HR) is an inward-directed light-driven halogen ion pump, and NpHR is a HR from *Natronomonas pharaonis*. Unphotolyzed NpHR binds halogen ion in the vicinity of the Schiff base, which links retinal to Lys256. This halogen ion is transported during the photocycle. We made various mutants of Thr218, which is located one half-turn up from the Schiff base to the cytoplasm (CP) channel, and analyzed the photocycle using a sequential irreversible model. Four photochemically defined intermediates (P_i, i = 1−4) were adequate to describe the photocycle. The third component, P_3, was a quasi-equilibrium complex between the N and O intermediates, where a N ↔ O + Cl^- equilibrium was attained. The $K_{d,N\leftrightarrow O}$ values of this equilibrium for various mutants were determined, and the value of Thr (wild type) was the highest. The partial molar volume differences between N and O, $\Delta V_{N\rightarrow O}$, were estimated from the pressure dependence of $K_{d,N\leftrightarrow O}$. A comparison between $K_{d,N\leftrightarrow O}$ and $\Delta V_{N\rightarrow O}$ led to the conclusion that water entry by the F-helix opening at O may occur, which may increase $K_{d,N\leftrightarrow O}$. For some mutants, however, large $\Delta V_{N\rightarrow O}$ values were found, whereas the $K_{d,N\leftrightarrow O}$ values were small. This suggests that the special coordination of a water molecule with the OH group of Thr is necessary for the increase in $K_{d,N\leftrightarrow O}$. Mutants with a small $K_{d,N\leftrightarrow O}$ showed low pumping activities in the presence of inside negative membrane potential, while the mutant activities were not different in the absence of membrane potential. The effect of the mutation on the pumping activities is discussed.

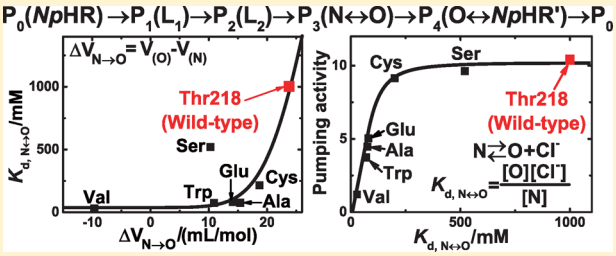

Halorhodopsin (HR) is a light-driven inward-directed Cl^- pump.[1−4] The movement of negative charge into the cytoplasm creates a negative interior membrane potential, which is a part of the proton-motive force, a driving force for energy transduction in biological membranes. Similar to the well-known light-driven outward-directed H^+ pump bacteriorhodopsin (BR), HR uses retinal as a chromophore, which binds to specific lysine residue of the last and seventh helix via a protonated Schiff base.[5] HR and BR that belong to the family of microbial rhodopsins show a photocycle. Absorption of light by retinal results in its isomerization from all-*trans* to 13-*cis* and initiates a photocycle in which the photoexcited state returns to the original pigment through various photointermediates with names such as K−O. During a photocycle, HR transports one Cl^- from the extracellular (EC) to the cytoplasmic (CP) space.

Since its discovery in the archaeon *Halobacterium salinarum*, various types of HRs have been reported. The most extensively studied are HR from *H. salinarum* (HsHR) and HR from *Natronomonas pharaonis* (NpHR). NpHR has advantages over HsHR. First, no light−dark adaptation of NpHR has been found,[6,7] and HsHR does show this adaptation.[8−10] Retinal isomers of HsHR in the dark are in an approximately 1:1 all-*trans*:13-*cis* ratio. Illumination increases the all-*trans* content, which decreases to the dark-adapted value during incubation in the dark. In contrast, for NpHR, all-*trans*-retinal is a major component independent of the light- or dark-adapted state. Second, the 13-*cis* pigment in NpHR does not have a detectable photocycle in contrast to HsHR.[7,9] Third, NpHR has been functionally expressed in *Escherichia coli* cells;[11,12] these cells have a much shorter doubling time than halobacterial cells. Functional expression of HsHR in *E. coli* cells has not been successful, although it was reported that active HsHR was obtained by solubilization of cells in the presence of excess retinal.[13] For all these reasons, we employed NpHR in this study.

The photocycle of NpHR has been investigated previously. In contrast to that of BR, the deprotonated Schiff base does not appear because the proton-accepting residue BR Asp85 is replaced with a non-proton-accepting threonine (Thr or T) for both HRs.[5] The photocycle scheme and pumping mechanism are still being debated. Ludmann et al.[14] described an NpHR → K ↔ L_1 ↔ L_2 ↔ N ↔ O ↔ NpHR′ → NpHR cycle. The absorption maxima (λ_{max}) are 580 nm for unphotolyzed NpHR, 585 nm for K, 530 nm for L (L_1 and L_2), 580 nm for N, and 615 nm for O.[7] NpHR′ has a λ_{max} that is almost the same as that of NpHR,[7] suggesting that its conformation may be only slightly different from that of the original NpHR. Essen proposed the conformational restoration of some residues

Received: September 18, 2013
Revised: December 1, 2013
Published: December 3, 2013

   dx.doi.org/10.1021/bi401295e | *Biochemistry* 2013, 52, 9257−9268

around Arg123 or a change in the orientation of Arg123 itself during the NpHR′ to NpHR transition.[15] Chizhov and Engelhard proposed a photocycle scheme[16] that exhibited two differences compared to that of Ludmann et al.: (1) the existence of two O intermediates, which were denoted O^1_{600} and O^2_{600}, and (2) the appearance of N after O (O^2_{600}). We analyzed the flash-induced absorbance changes of NpHR using an irreversible sequential model[17] that was originally introduced by Chizhov et al.[18]

$$P_0 \rightarrow P_1 \rightarrow P_2 \rightarrow P_n \rightarrow P_0 \quad (1)$$

where P_0 stands for the unphotolyzed pigment and P_i ($i = 1-n$) terms stand for the photochemically defined intermediates, which are kinetically distinguishable in the analysis according to this irreversible transition model. The P_i intermediates may contain a few physically defined intermediates such as L, N, and O when the reverse reactions exist between them. "Physically defined" means that these intermediates are spectrally distinguishable because of their physical differences. The assignment and name of the intermediates are usually based on BR nomenclature. Here, n is the smallest number of photochemically defined intermediates required to adequately simulate the data. We found that an n of 4 is sufficient,[17] and we determined the spectra of P_i ($i = 1-4$). Note that, using our apparatus, the K intermediate is not clearly observable, so exactly five photochemically defined intermediates are necessary. From the spectra of the estimated P_i we identified P_1-P_4 as L_1, L_2, a quasi-equilibrium complex of N and O, and a quasi-equilibrium complex of a red-shifted species [potentially O (see the scheme of Ludmann et al.[14])] and NpHR′, respectively. On the basis of comparison with the scheme of Ludmann et al.,[14] we describe our scheme as follows: NpHR → K → L_1 → L_2 → (N ↔ O) → (O ↔ NpHR′) → NpHR. The parentheses indicate the quasi-equilibrium complexes. The equilibrium of (O ↔ NpHR′) shifted greatly to NpHR′ because only small amounts of O were observed. Other reports have also proposed the existence of two L intermediates.[9,16,19,20] Our scheme indicates that in the scheme of Ludmann et al.,[14] the rates of L_2 → L_1 and N → L_2 transitions are negligible. Ludmann et al.[14] calculated the time-dependent concentrations of the respective photointermediates and revealed a time course of N and O content similar to that proposed in our scheme.

Váró et al. found that the rate constants of both O → NpHR′ and O → N transitions were dependent on the external Cl^- concentration, suggesting that O decay accompanies uptake of Cl^- from the outside and that O is a Cl^--free form,[21] which is possible on the basis of its absorption maximum. Supporting evidence was obtained from transient grating measurements[22] and from the absorbance changes of bacterioruberin, an intrinsic membrane potential indicator of the halobacterial cell membrane (manuscript in preparation). Lanyi and Vodyanoy[23] and Ames et al.[24] assumed that O in HsHR was in a Cl^--free form. Fourier transform infrared (FTIR) spectroscopy also concluded that O in NpHR is a Cl^--free form.[25] In our analysis that adopted the N−O equilibrium, the following equilibrium equation holds:

$$N \leftrightarrow O + Cl^- \quad (2)$$

where the dissociation constant of Cl^- ($K_{d,N\leftrightarrow O}$) is described as

$$K_{d,N\leftrightarrow O} = \frac{[O][Cl^-]}{[N]} \quad (3)$$

After Cl^- release during the formation of O, the subsequent Cl^- uptake is considered to occur during the O → NpHR′ transition. This notion is consistent with the Cl^--dependent acceleration of the O → NpHR′ transition described above[21] and the closely resembled absorption spectra between NpHR′ and the initial dark state.[16,17,21] Contrary to this notion, the experiments that assessed the NpHR-induced electrogenicities did not detect the Cl^- movement assigned to the Cl^- uptake during this transition.[14] Thus, the details of Cl^- uptake are still under debate.

Several functionally important amino acid residues have been reported on the basis of mutagenesis experiments.[26−32] Of the residues in the EC channel, NpHR Arg123, Thr126, and Ser130, which correspond to HsHR Arg108, Thr111, and Ser115, respectively, were found to be important. These residues constitute the Cl^- binding site in the dark, and their mutation inhibited Cl^- binding and/or distorted the photocycle. The putative important residues in the Cl^--interacting (binding) site in the CP channel are Lys215 and Thr218, corresponding to HsHR Arg200 and Thr203, respectively.[27,30,33] These residues are hydrophilic or relatively hydrophilic compared to the large population of hydrophobic residues in the CP channel. Thr218 is located approximately only one helix turn from the Schiff base. Previously, we mutated this residue to Val and found significant changes in the photocycle: The O intermediate became hardly measurable.[30] The importance of this residue in HsHR was also reported by Rüdiger and Oesterhelt.[27] For HsHR, the replacement with Val slowed the turnover of the photocycle and thereby reduced the Cl^- transport activity. Because of the proximity of the Schiff base, Kolbe et al. proposed that the Cl^- probably forms a hydrogen bond with the OH group of the Thr after the passage of Cl^- over the Schiff base.[33]

In this study, we mutated Thr218 to a variety of amino acid residues and measured changes in the Cl^--dependent N/O intermediate ratio (determination of $K_{d,N\leftrightarrow O}$ in eq 3). Needless to say, a large $K_{d,N\leftrightarrow O}$ indicates a low affinity for Cl^-. The partial molar volume changes between N and O ($\Delta V_{N\rightarrow O}$) were estimated from the pressure dependence of $K_{d,N\leftrightarrow O}$. The volume change might be due to water entry at O as observed for the M-to-N transition of BR.[34] The values of both $K_{d,N\leftrightarrow O}$ and $\Delta V_{N\rightarrow O}$ were the largest for the wild type and T218S mutant, and the relationship between $K_{d,N\leftrightarrow O}$ and $\Delta V_{N\rightarrow O}$ proposed the formation of a special coordination of the entered water molecule with the OH group of Thr or Ser. Rate constants k_2 and k_3 are those of the formation of the N−O complex and its decay, respectively. These values were also largest for the wild type and the serine mutant. Thus, Thr (wild type) is best suited to the transfer of Cl^-. The effect of the mutation on NpHR activity is also discussed.

MATERIALS AND METHODS

Construction of Expression Plasmids of Mutants with a Histidine Tag. Plasmids for the expression of various Thr218 mutants were constructed with a Quikchange site-directed mutagenesis kit (Stratagene, Agilent Technologies, Tokyo, Japan) and a modified pET-21c(+) vector (Merck Japan, Tokyo, Japan) to create a histidine-tagged region. The mutations introduced were confirmed by a standard method using an automated DNA sequencer (model 3100, Applied Biosystems, Foster City, CA). The expression of the recombinant NpHR in *E. coli* cells [strain BL21(DE)] and the solubilization procedure were described previously.[12]

Fractions of the proteins separated with a Ni-NTA agarose (Qiagen, Hilden, Germany) column were collected by elution with buffer E [50 mM Tris-HCl (pH 7.0), 400 mM NaCl, 150 mM imidazole, and 0.1% *n*-dodecyl β-D-maltopyranoside (DDM) (Dojindo Laboratory, Kumamoto, Japan)]. The samples were then placed in appropriate buffer solutions by being passed over Sephadex-G25 in a PD-10 column (GE Healthcare Japan, Tokyo, Japan).

Flash Photolysis Spectroscopy under Normal Pressure. The computer-controlled flash photolysis apparatus used was the same as that reported previously.[30] The transient absorption changes (λ from 410 to 710 nm, every 10 nm) induced by a light pulse (λ = 532 nm, 7 ns, ~5 mJ) of a Q-switched Nd:YAG laser (Surelite I-10; Continuum, Santa Clara, CA) were acquired every 0.5 μs between −44 and 218 ms. At each selected wavelength, 30 laser pulses were used to improve the signal-to-noise ratio. Data points on a logarithmic time scale were picked from the observed data for the following analysis. The temperature was kept constant by circulating thermostated water at 25 °C. The NpHR concentration was 10−15 μM, which was determined using an extinction coefficient of 54000 at 580 nm. Experiments were performed with varying concentrations of Cl^-, whereas the ionic strength was maintained equivalent to 4 M NaCl through the use of appropriate concentrations of Na_2SO_4 for both the normal and the following high-pressure experiments. The pH of the sample was 6.0 and buffered using 10 mM MES.

Flash Photolysis Spectroscopy under High Pressure. The pressure cell used was the same as that reported previously.[35] Using a hand-operated hydraulic pump, the pressure on the sample was changed between 1 and 1480 bar using water as the pressure medium. The pressure applied was determined by a manometer. The actinic laser flash was from the same Nd:YAG laser described above. The other experimental conditions were the same as those under normal pressure.

Analysis of Flash Photolysis Data. As described in the introductory section, we employed an irreversible sequential model and found that an n of 4 was sufficient to simulate the data.[17] This means that the NpHR photocycle can be described by the following sequential scheme:

$$P_0 \rightarrow P_1 \rightarrow P_2 \rightarrow P_3 \rightarrow P_4 \rightarrow P_0 \quad (4)$$

As described above, the K intermediate is not detected in our apparatus because of the slow response. Judging from the determined decay rate constants, our P_1−P_4 may correspond to P_3−P_6, respectively, in the analysis by Chizhov and Engelhard.[16] In this assignment, our P_3 corresponds to P_5 of Chizhov and Engelhard. The spectra of these two intermediates show similar Cl^- dependence as described below. Further analysis was performed as described previously[17,18,30] (also see the Supporting Information). Briefly, using the fitting results, the rate constant of the decay of the P_i state (k_i) and the absorption differences between P_i and P_0 ($\Delta\varepsilon_i$) were calculated. Independently, the measured spectrum of the P_0 state was fit with the following four factors: (1) skewed Gaussian (SG) function[18] of the main absorption band at approximately 580 nm, (2) the background scattering ($A + B/\lambda^4$; λ in nanometers), (3) SG function of the β-band at approximately 400 nm, and (4) SG function of the band from the aromatic residues at approximately 280 nm. The SG function is defined by four parametersL λ_{max} (in nanometers), A_{max} (amplitude at λ_{max}), ρ (skewness of the absorption band), and $\Delta\nu$ (half-bandwidth in inverse centimeters). The sum of the SG functions of parts 1 and 3 expresses the retinal spectrum of the P_0 state. Typical parameter values were as follows: λ_{max} = 575 nm, ρ = 1.62, and $\Delta\nu$ = 3152 cm^{-1} for the SG function of part 1, and λ_{max} = 392 nm, ρ = 1.70, and $\Delta\nu$ = 8210 cm^{-1} for the SG function of part 3. The relative A_{max} value of SG function 3 and 1 was approximately 0.11. By adding this retinal spectrum to the absorption difference ($\Delta\varepsilon_i$), we obtained the absolute spectra of the P_i state. Further details of this method have been described previously.[17,30]

Decomposition of the Spectra of the P_3 State. As described previously[17] and below (Results), P_3 was a quasi-equilibrium mixture of N and O whose relative fractions depended on the Cl^- concentration (see eqs 2 and 3). In addition to the respective main absorption bands, the P_3 intermediate spectra included the respective β-bands. Assuming both β-bands are identical with that of the P_0 state, the P_3 spectrum is expressed as

$$\text{spectrum of } P_3 = f \times \text{Abs}(N, \lambda) + (1 - f) \times \text{Abs}(O, \lambda) + \text{Abs}(\beta, \lambda) \quad (5)$$

where f, Abs(N,λ), Abs(O,λ), and Abs(β,λ) stand for the fraction of N in the P_3 state, the main band of N, the main band of O, and the β-band, respectively. By employing the SG functions to express the three absorption bands, we decomposed the P_3 spectra to estimate f. In this calculation, we assumed f to be the only parameter varying with the Cl^- concentration. Typical parameter values of SG functions were as follows: λ_{max} = 518 nm, A_{max} = 0.65, ρ = 2.07, and $\Delta\nu$ = 4348 cm^{-1} for Abs(N,λ), and λ_{max} = 607 nm, A_{max} = 0.87, ρ = 1.74, and $\Delta\nu$ = 3509 cm^{-1} for Abs(O,λ). The A_{max} values described above are relative to the A_{max} for the main absorption band of the P_0 state.

Determination of $K_{d,N\leftrightarrow O}$ of the Wild Type and Mutants. Values of f and $1 - f$ (fractions of N and O in the P_3 state, respectively) were plotted against Cl^- concentration. In these plots, the two curves crossed each other at f = 0.5 (see Figure 2). The concentration of Cl^- giving f = 0.5 is $K_{d,N\leftrightarrow O}$. For some mutants, another method was adopted. The details are described in the Supporting Information.

NpHR Activity Measurements by Photoinduced Proton Transfer. The activities of various mutants were estimated using *E. coli* suspensions. Cl^- transport by NpHR hyperpolarizes the cell membrane and causes passive H^+ uptake. Thus, the activity is evaluated as the pH increase of the suspension. It is worth noting that we used fresh cells without carbonyl cyanide *m*-chlorophenylhydrazone (CCCP). The rationale for this is described elaborately in the Discussion. For these experiments, all procedures were performed as quickly as possible. The *E. coli* cells were harvested at 3600*g* for 5 min at 4 °C and washed twice with a cold unbuffered basal solution containing 150 mM NaCl, 50 mM $MgSO_4$, 40 mM KCl, and 0.5 mM $CaCl_2$. Concentrated cell suspensions were obtained. For activity measurements, the original suspensions were diluted with the basal solution. The cuvette was thermostated at 25 °C and the sample volume was 1.5 mL. The pH was measured with a glass electrode, and the initial pH values of the samples were ~6.5. Illumination was provided with a 590 ± 8.5 nm LED (LXHL-LL3C, Philips Lumileds Lighting Co., San Jose, CA). Within 3−5 min of illumination, the pH increase became saturated. After each measurement, the pH increase was calibrated to the amount of protons taken up

dx.doi.org/10.1021/bi401295e | *Biochemistry* 2013, 52, 9257−9268

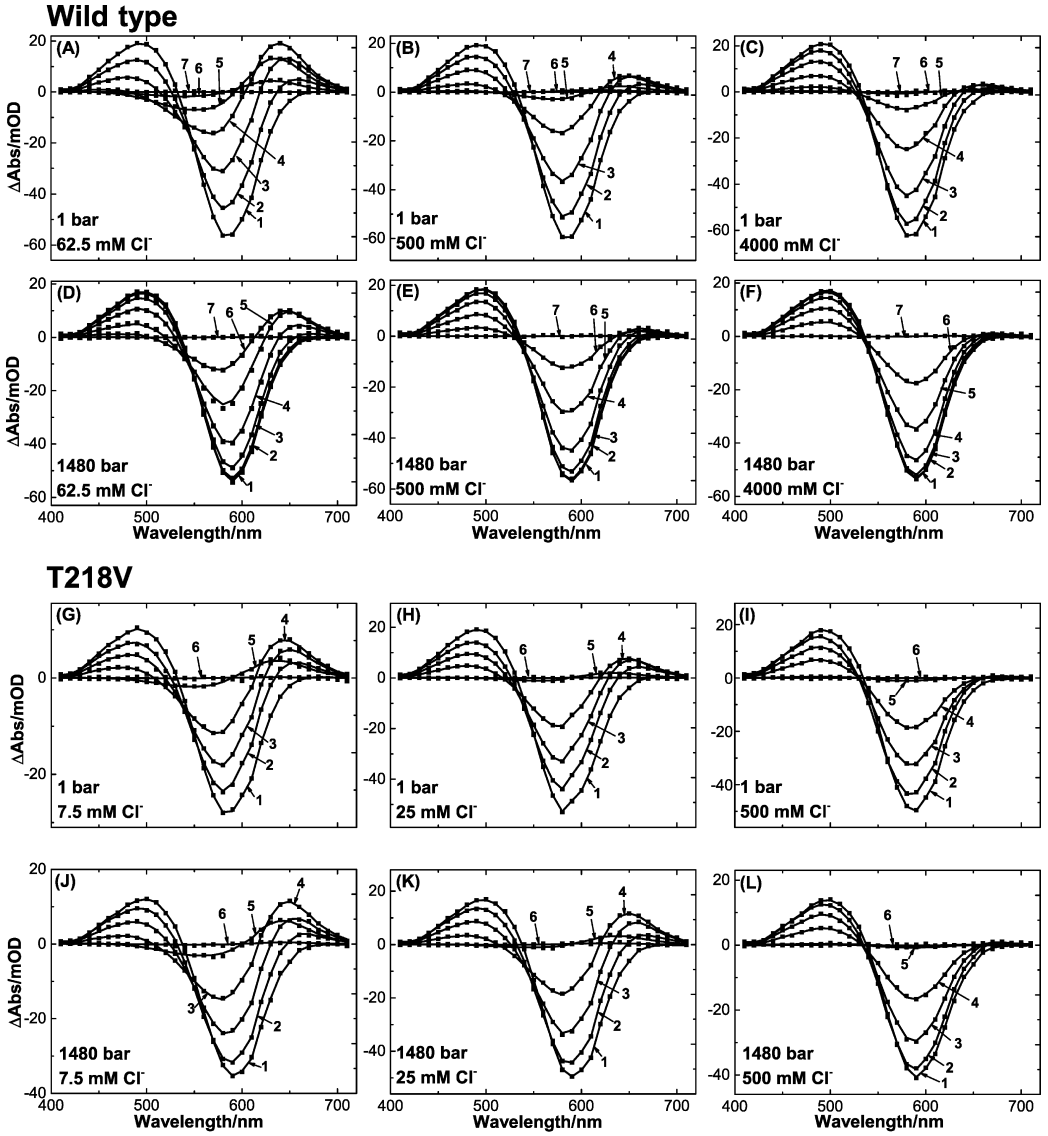

Figure 1. Good agreement of observed and simulated flash-induced light minus dark difference spectra. Filled symbols show the observed spectra. The best results from the fitting analysis (see eq S1 and the Supporting Information) are shown with lines. The top row (A–C) shows the wild-type data at 62.5 (A), 500 (B), and 4000 mM Cl^- (C) under 1 bar. The concentrations of the three panels in the second row (D–F) are the same as those of the top row (A–C, respectively), but the pressure is 1480 bar. The times of the data after the flash are as follows: 1, 0.09 ms; 2, 0.32 ms; 3, 0.63 ms; 4, 1.17 ms; 5, 2.23 ms; 6, 4.23 ms; 7, 29.4 ms. The panels in the third and fourth rows show the data from T218V. The Cl^- concentrations of panels G and J are 7.5 mM, those of panels H and K 25 mM, and those of panels I and L 500 mM. The third row depicts the data under 1 bar, and the panels in the fourth row depict data under 1480 bar. The times of the data after the flash for T218V are as follows: 1, 0.32 ms; 2, 2.23 ms; 3, 4.25 ms; 4, 8.11 ms; 5, 29.4 ms; 6, 106 ms.

into the cells by adding a known amount of HCl. To determine the relative pigment concentrations in the cuvette, the flash photolysis yields at 580 nm were recorded for the original cell suspensions. Compared with the pH values of the de-energized cells (see below), the light-induced pH increases were small, and accurate measurements were difficult to obtain because of relatively large baseline fluctuation. Thus, the pH measurements were performed for five to eight samples diluted at various times from the original cell suspensions. The diluted samples had optical densities at 660 nm (OD_{660}) of 0.1–1.3. The calibrated amounts of proton uptake were plotted against the relative pigment concentrations, which are the products of the flash yields and the dilution ratios. The slopes of the plots indicate the relative Cl^- pumping activities of the pigments. Independently, the proton uptake experiments were also performed using de-energized cells. For these experiments, washed cells were shaken gently for 2 h at 25 °C in the presence of 10 μM CCCP. After that, the cells were washed again and diluted to an OD_{660} of 0.5 with the basal solution supplemented with 10 μM CCCP. The light-induced pH changes were relatively large. Thus, pH measurements were performed for only the samples at an OD_{660} of 0.5. The relative pigment concentrations were also determined from the flash photolysis yields for original concentrated cell suspensions and the dilution ratios. The proton uptake was proportional to the pigment concentration. The relative pumping activities, which are comparable to those of the intact cells, were determined by dividing the proton uptake by the relative pigment concentration.

dx.doi.org/10.1021/bi401295e | *Biochemistry* 2013, 52, 9257–9268

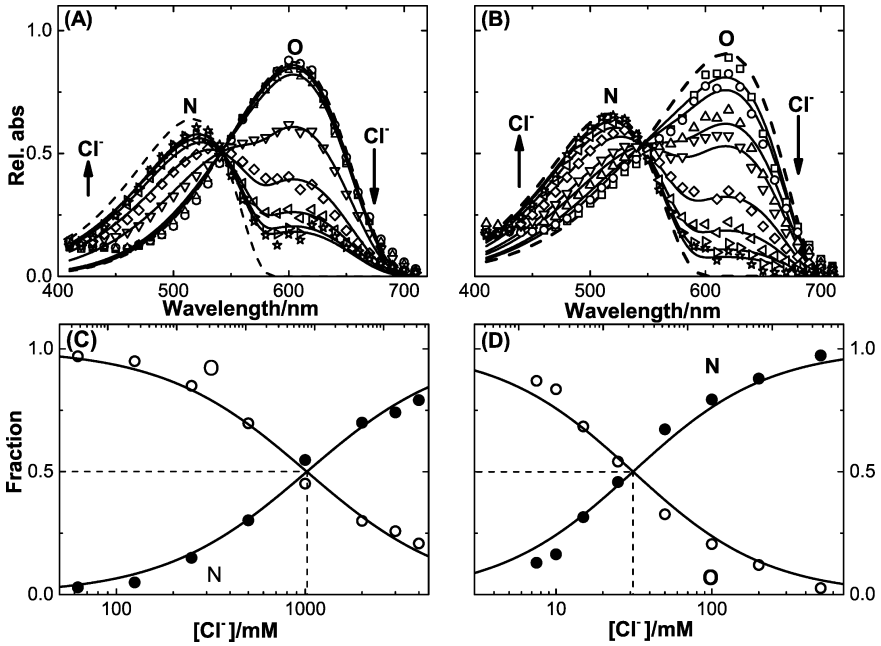

Figure 2. Determination of $K_{d,N\leftrightarrow O}$. Symbols in panels A and B show the P_3 spectra of the wild type (A) and T218V (B) at Cl^- concentrations of 62.5 (□), 125 (○), 250 (△), 500 (▽), 1000 (◇), 2000 (left-pointing triangle), 3000 (right-pointing triangle), and 4000 mM (☆) for the wild type and 7.5 (□), 10 (○), 15 (△), 25 (▽), 50 (◇), 100 (left-pointing triangle), 200 (right-pointing triangle), and 500 mM (☆) for T218V. Solid lines are the calculated best-fit curves from eq 5. The determined spectra of N and O are shown by broken lines in panels A and B, and their fractions are plotted in panels C (wild type) and D (T218V) against the Cl^- concentration. Two curves in panels C and D cross each other at $f = 0.5$, at the $K_{d,N\leftrightarrow O}$ concentration.

RESULTS

Agreement of the Observed Flash-Induced Transient Absorbance Changes with Simulation Curves Using $n = 4$ in eqs 1 and 4. Previously, we showed that the photocycle of NpHR was adequately described with four photochemically defined intermediates.[17] This was also valid in the experiments described here using various mutants and high pressures. Figure 1 shows some examples of the excellent agreement between the observed flash-induced light minus dark difference spectra and the simulated curves described by the sum of four exponential functions, which assume the existence of four photochemically defined intermediates (P_i, where $i = 1-4$). Using the determined fitting parameters, the absolute spectra of P_i ($i = 1-4$) were calculated as described previously.[17,30] The calculated spectra and the related data are shown in Figure S1 of the Supporting Information. In Figure 1, the top row (panels A–C) shows the data from the wild type at 62.5 (A), 500 (B), and 4000 mM Cl^- (C) under 1 bar. The concentrations of the three panels in the second row (D–F) are the same as those in the top row (A–C, respectively), but the pressure is 1480 bar. The panels in the third and fourth rows are the data from the T218V mutant. The concentrations of panels G and J are 7.5 mM Cl^-, those of panels H and K 25 mM Cl^-, and those of panels I and L 500 mM Cl^-. The third row depicts the data under 1 bar, and the panels in the fourth row depict data under 1480 bar. The differences in the Cl^- concentration of the wild-type protein and the T218V mutant are due to the differences in $K_{d,N\leftrightarrow O}$ in eq 3.

These 12 panels indicate that with an increase in Cl^- concentration, the amounts of photoproducts at the longer wavelength (maybe O intermediate) decrease, which agrees with the equilibrium equation of eq 2. For the wild-type protein (panels A–F), an increase in pressure results in a lower yield of the long-wavelength product, O, whereas the T218V intermediate shows the opposite tendency (panels G–L). This is because the opposite partial molar volume changes between N and O for these two species (see below).

Estimation of $K_{d,N\leftrightarrow O}$ Values for the Wild-Type Protein and Various Mutants under Normal Pressure. The spectra of P_3 are composed of a quasi-equilibrium mixture of N and O,[17] which have typical λ_{max} values of 516 and 607 nm, respectively. The symbols in panels A and B of Figure 2 show the P_3 spectra for the wild type (A) and T218V (B) at varying Cl^- concentrations. Here, the absorbances are shown when P_0 is taken to be unity. The level of the longer-wavelength product (O) decreases with an increase in Cl^- concentration, whereas the levels of the shorter-wavelength products (N) increase. For these P_3 spectra, we performed the fitting analyses according to eq 5. The solid lines denote the best-fit curves. This analysis simultaneously determines the spectra of pure N [Abs(N,λ)] and O [Abs(O,λ)] and the fraction of N (f). The fraction of O is given by $1 - f$. The dashed lines in panels A and B denote the determined spectra of pure N and O. The fractions of N and O are plotted in panel C for the wild type and in panel D for T218V. Empty circles indicate the O fraction, and filled circles indicate the N fraction. These two lines cross each other at $f = 0.5$, and the concentrations at these points are the $K_{d,N\leftrightarrow O}$. T218V has a much smaller $K_{d,N\leftrightarrow O}$ than the wild-type protein. The $K_{d,N\leftrightarrow O}$ values of wild type and various mutants were also determined from the linear relationships between $\log[(1-f)/f]$ and $\log[Cl^-]$ (Figure S2 of the Supporting Information). The details are given in the Supporting Information. The determined values are almost the same as those described above. Thus, $K_{d,N\leftrightarrow O}$ values of some mutants were determined by the latter procedure. The $K_{d,N\leftrightarrow O}$ values for Gln, Met, Phe, Ile, and Leu mutants were not able to be estimated because their $K_{d,N\leftrightarrow O}$ values were very small (less than ~5 mM); using

dx.doi.org/10.1021/bi401295e | Biochemistry 2013, 52, 9257–9268

these dilute solutions, we could not distinguish their photocycle from that of the Cl^--free form. The estimated values of $K_{d,N\leftrightarrow O}$ are listed in Table 1 with the hydropathy index of the amino acid at position 218. The value of $K_{d,N\leftrightarrow O}$ for the wild type (Thr) is the largest.

Table 1. $K_{d,N\leftrightarrow O}$ and $\Delta V_{N\rightarrow O}$ for Various Mutants at Position 218 and Hydropathy Indices of the Mutated Residue

amino acid residue at position 218	hydropathy index[b]	$K_{d,N\leftrightarrow O}$ (mM) at 1 bar	$\Delta V_{N\rightarrow O}$ (mL/mol)
Glu (E)	−0.74	80	14.1
Ser (S)	−0.18	526	7.7
Thr (T)[a]	−0.05	1000	23.7
Cys (C)	0.29	215	19.7
Ala (A)	0.62	75	14.8
Trp (W)	0.81	70	10.9
Val (V)	1.08	30	−9.6

[a]The wild type. [b]From ref 50.The $K_{d,N\leftrightarrow O}$ values of the Gln, Met, Phe, Ile, and Leu mutants were not estimated. Their $K_{d,N\leftrightarrow O}$ values were very small (less than ∼5 mM), so that we could not distinguish the photocycle from that of the Cl^--free form.

Rate Constant Dependence on the Chloride Concentration. Figure 3 shows the observed rate constants of the wild-type protein [Thr (T)] and various mutants under normal pressure. Panels are arranged in order from hydrophilic (left) to hydrophobic (right) amino acid residues at position 218. The rate constant k_1 (□) is that of the transition from P_1 (L_1) to P_2 (L_2) and is faster than other rate constants for all mutants and the wild-type protein. They seem to be independent of Cl^- concentration, implying that this process proceeds without interaction with Cl^- in the medium. Although the molecular event underlying this transition is not clear at present, the following data have been reported. FTIR showed a change in the amide I/II vibration mode in NpHR,[36] and low-temperature FTIR showed changes in the protein and water O−H stretching bands in HsHR[20] and the deprotonation of Glu234 at the EC surface in NpHR.[37] k_2 (○) is the rate constant of the P_2 (L_2) to P_3 (N ↔ O) transition, and values increase roughly linearly with an increase in the external Cl^- concentration (logarithmic scale), suggesting the necessity of the presence of external Cl^-. The binding of this ion might need to occur for the P_2 to P_3 transition to proceed. k_3 (×) is the rate constant of the P_3 (N ↔ O) to P_4 (O ↔ NpHR′) transition, in which the external Cl^- enters from the EC channel to bind at the binding site near the Schiff base, because the main component of P_4 is NpHR′. Therefore, these rates should increase with an increase in the external Cl^- concentration. However, the data show a convex curve that is a function of Cl^- concentration. One plausible reason will be discussed below. The appearance of O in both P_3 (N ↔ O) and P_4 (O ↔ NpHR′) implies that two O intermediates exist, as proposed by Chizhov and Engelhard.[16] They denoted them as O^1_{600} and O^2_{600}, respectively, and proposed a concept that, during the O^1_{600} to O^2_{600} transition, the accessibility changes from the CP to EC channel. The value of k_4 (▽) is the rate of the transition from P_4 (O ↔ NpHR′) to NpHR (the original pigment). Except for the wild type (Thr), the rate does not depend on the external Cl^- concentration. The molecular nature of this transition is not clear at present, as mentioned above.

Partial Molar Volume Changes between N and O. Because we assume equilibrium between N and O in P_3, the pressure dependence of $K_{d,N\leftrightarrow O}$ results in partial molar volume changes in accordance with eq 6.

$$\left(\frac{\partial \log K_{d,N\leftrightarrow O}}{\partial P}\right)_T = -\frac{\Delta V_{N\rightarrow O}}{2.3RT} \quad (6)$$

where $\Delta V_{N\rightarrow O}$ is the partial molar volume change between N and O with reference to that of N, P is the hydrostatic pressure, R is the gas constant, and T is the absolute temperature. This equation describes the pressure-dependent shift of the N−O equilibrium governed by Le Chatelier's principle: the application of the pressure shifts the equilibrium toward the state having a smaller volume. In Figure 4, log $K_{d,N\leftrightarrow O}$ is plotted versus pressure. The slope gives $\Delta V_{N\rightarrow O}$ (values listed in Table 1). The contribution of the Cl^- volume is not taken into account because the values for all mutants and the wild type should be the same. The $K_{d,N\leftrightarrow O}$ values under high pressure were determined to be the same as those under normal pressure (see Figure 2). Only the T218V mutant shows a negative value; the others are positive. In Figure S3 of the Supporting Information, the P_i spectra of the wild-type protein

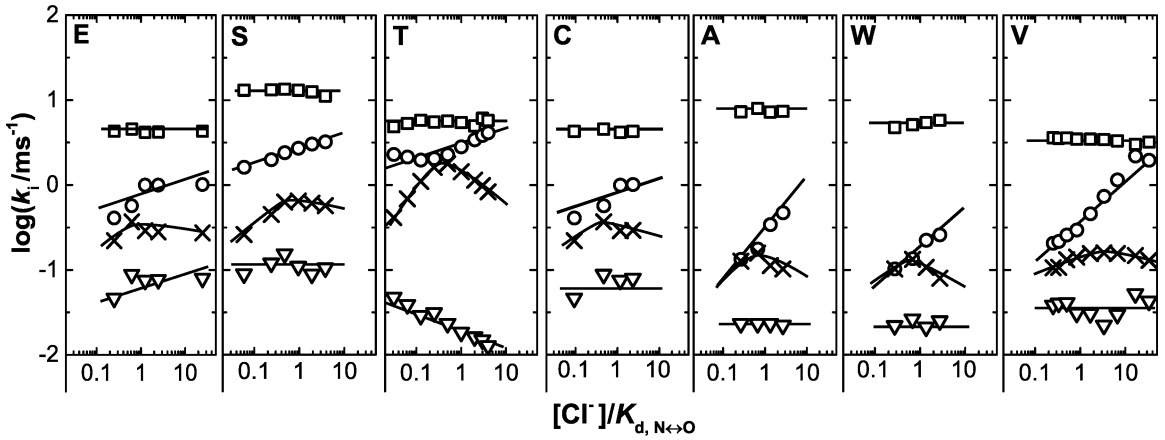

Figure 3. Cl^- concentration dependence of k_i. The Cl^- concentrations are expressed as $[Cl^-]/K_{d,N\leftrightarrow O}$ (the $K_{d,N\leftrightarrow O}$ values of the wild type and mutants are listed in Table 1). k_1 (□) is the rate constant of the transition from P_1 (L_1) to P_2 (L_2). k_2 (○) is the rate constant of the P_2 (L_2) to P_3 (N ↔ O) transition. k_3 (×) is the rate constant of the P_3 (N ↔ O) to P_4 (O ↔ NpHR′) transition. k_4 (▽) is the rate of the transition from P_4 (O ↔ NpHR′) to NpHR (the original pigment). The behavior of k_3 is discussed in the Discussion.

dx.doi.org/10.1021/bi401295e | Biochemistry 2013, 52, 9257−9268

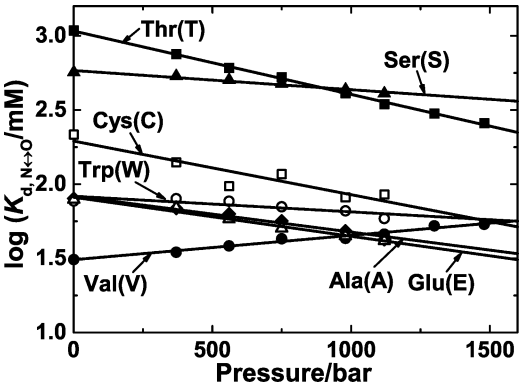

Figure 4. Pressure dependence of $K_{d,N\leftrightarrow O}$. According to eq 6, the slopes give $\Delta V_{N\rightarrow O}$ (values of which are listed in Table 1).

and T218V under various pressures are shown. The P_3 spectra indicate the reverse pressure dependence of N and O components for the wild type and T218V. P_1, P_2, and P_4 show a small pressure dependence.

Pumping Activities of the Wild-Type Protein and Various Mutants. The pumping activities were measured by the proton uptake under constant illumination with a glass pH electrode. Intact cells were used. The preparation (harvest and washing) of cells was conducted as quickly as possible in the cold. The photoinduced proton movements were measured in the absence of CCCP, under which condition the cells have interior negative membrane potential. The results are shown in Figure 5. The abscissa is the relative pigment concentration in

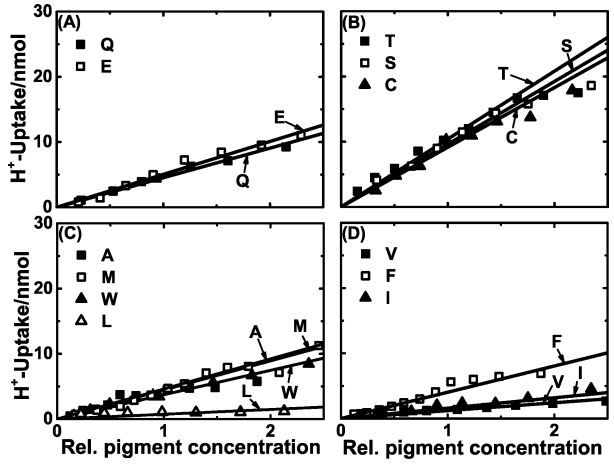

Figure 5. Pumping activities measured by photoinduced proton uptake. Amounts of photoinduced proton uptake are plotted vs the relative concentrations of pigments that were estimated from flash photolysis yields. Intact cells were used, and measurements were taken in the absence of the protonophore CCCP. The medium consisted of 150 mM NaCl, 50 mM $MgSO_4$, 40 mM KCl, and 0.5 mM $CaCl_2$. For the sake of clarity, the results are shown in four separate panels. The slopes represent the pumping activities.

the cuvette, which was estimated by the 580 nm flash yields of the original concentrated cell suspensions (see Materials and Methods for details). For the sake of clarity, the results are shown in four panels. The slopes of the lines in Figure 5, which represent relative pumping activities, are indicated in the histogram in Figure 6A, where the plots are arranged in order from hydrophilic (left) to hydrophobic (right) amino acid residues at position 218. The wild type (T) shows the largest

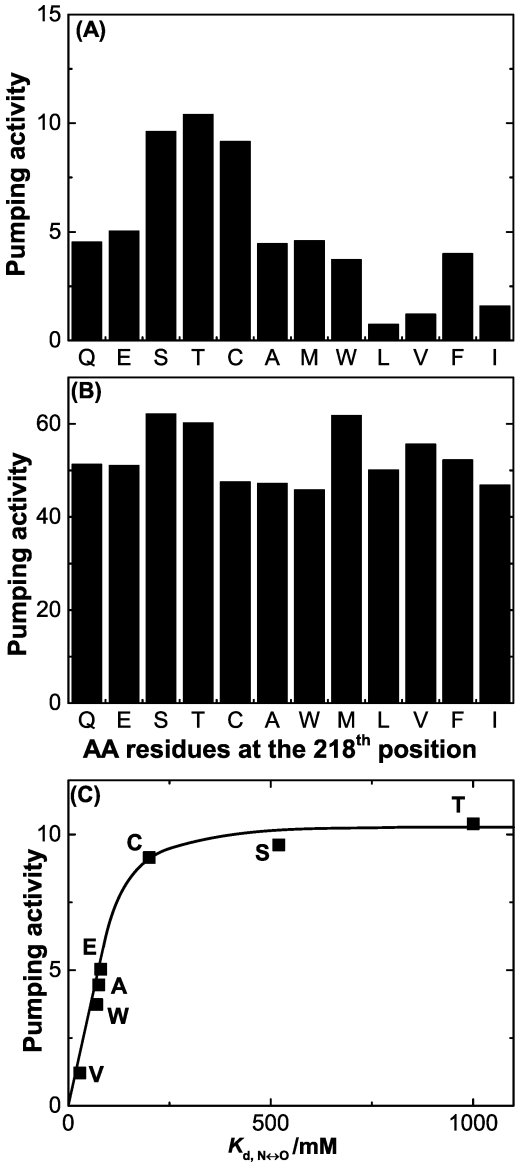

Figure 6. Correlation between $K_{d,N\leftrightarrow O}$ and pumping activity in the presence or absence of membrane potential. (A) The values of the slopes in Figure 5, which represent the pumping activities, are shown as a histogram. (B) Corresponding histogram for the de-energized cells in the presence of 10 μM CCCP. It is noteworthy that all mutants show similar magnitudes, in contrast to the results in panel A. (C) Plot of the pumping activities of intact cells (panel A) vs $K_{d,N\leftrightarrow O}$. The relative pumping activity increases with an increase in $K_{d,N\leftrightarrow O}$.

activity. The Q, M, L, F, and I mutants are not listed in Table 1, but the activities are shown here. Note that the $K_{d,N\leftrightarrow O}$ values of these mutants were very small (<5 mM). Neither $K_{d,N\leftrightarrow O}$ nor $\Delta V_{N\rightarrow O}$ was estimated because of the contamination of the Cl^--free photocycle. In these experiments, however, all pigments are the Cl^--bound form because the medium in this experiment contained approximately 190 mM Cl^-. In Figure 6C, the pumping activities are plotted against $K_{d,N\leftrightarrow O}$, indicating that the activities increase with an increase in $K_{d,N\leftrightarrow O}$.

We also measured pumping activities using de-energized cells. These cells were prepared by being gently shaken for 2 h in the presence of CCCP. The main difference between intact and de-energized cells is the presence or absence of the membrane potential. Interestingly, the pumping activities by

dx.doi.org/10.1021/bi401295e | *Biochemistry* 2013, 52, 9257−9268

de-energized cells are almost equal to one another (see Figure 6B). The intriguing effect of the negative interior membrane potential will be discussed below. Proton uptake measurements for de-energized cells were performed only for samples at an OD_{660} of 0.5. In Figure 6B, the activities are indicated by the proton uptake divided by the pigment concentration (see Materials and Methods for details). These activities correspond to the slopes of Figure 5 and thus are comparable with the plots in Figure 6A. The smaller activities of the intact cells are due to the uphill transport in the intact cells.

DISCUSSION

Cl^- Position in Each Photointermediate. As described above, O is a Cl^--free form in which Cl^- is released into the CP space. Because N and O are in quasi-equilibrium, it is natural to consider that at the N state, Cl^- is in the CP channel. There is supporting evidence for this assumption. A NpHR mutant engineered to bind with the NpHtrII (halobacterial transducer II from *N. pharaonis*) appreciably decreased the pumping activity by the complex, and no N was found in the photocycle of the complex.[17] In sensory rhodopsins I and II (SRI and SRII, respectively, also called phoborhodopsin), pigment proteins themselves have photoinduced H^+ pumping activity, but the complexes with the Htr (halobacterial transducer) lose activity.[38,39] This is interpreted in terms of "CP channel closure". Protons are considered to circulate only within the EC channel. Similarly, in the NpHR–NpHtrII complex, illumination may induce the circulation of Cl^- within the EC channel, resulting in no transport activity and no appearance of the N intermediate. Muneyuki et al. showed that charge (probably negative charge of Cl^-) movement occurred during the formation and decay of N.[40] The N to O transition is the process of releasing Cl^- from the protein, and the production of electrogenicity at the N decay is then conceivable. Another conclusion of Muneyuki et al.[40] was electrogenicity upon formation of the N state. This might be considered the translocation of Cl^- from EC to CP across the Schiff base from the precursor to N because Cl^- is located in the vicinity of retinal in the EC channel in the unphotolyzed state. The X-ray structure of L_1 of HsHR revealed that Cl^- remained in the EC channel.[41] Low-temperature FTIR of HsHR showed that Cl^- stayed in the EC channel near the Schiff base at both L_1 and L_2.[20] The three possibilities regarding the timing of the movement of Cl^- across retinal are the K to L_1, L_1 to L_2, and L_2 to N transitions. The observations described above suggest strongly that during the transition from L_2 to N, Cl^- moves from EC to CP across retinal. From an electrogenicity experiment using an NpHR-entrapped gel, Ludman et al. located the "extracellular-to-cytoplasmic switch" at the L_2 to N step,[14] which is consistent with our assumption. The presence of negative charge (Cl^-) in the vicinity of retinal in the CP channel at N is similar to the case of N of BR in which deprotonated Asp96 is located in the CP channel.

k_2 [transition of L_2 to the (N ↔ O) complex] and k_3 [transition of the (N ↔ O) complex to NpHR′] Are Largest for the Wild Type. Although Figure 3 shows the rate constants of k_i (i = 1–4), only k_2 and k_3 at the $K_{d,N\leftrightarrow O}$ are shown in Figure 7. Note that the ordinate scale is logarithmic in Figure 3. The rate constant for the transition from L_2 to the (N ↔ O) complex is k_2, and those of the wild-type (T) and Ser mutant are the largest. As described above, in this process, we assume that Cl^- transfers from EC to CP across the Schiff base. Thr or its Ser homologue may interact with Cl^- to generate

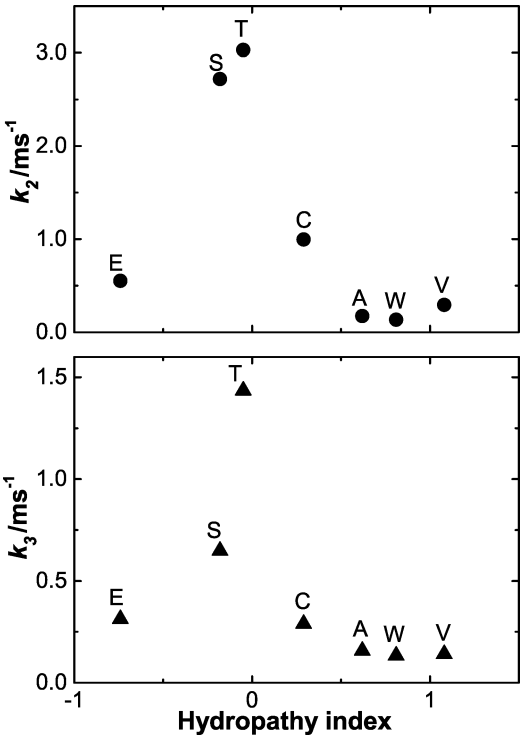

Figure 7. Plots of k_2 and k_3 at $K_{d,N\leftrightarrow O}$ vs the hydropathy index of the residue at position 218. Those of the wild type (T) and Ser (S) mutant are the largest.

prompt N formation, and the OH group of the residue may be important. It is noted that in the dark state of NpHR, Cl^- interacts with the OH group of Ser130 and Thr126 as well as with one water molecule and the protonated Schiff base.[42] The importance of Ser130 and Thr126 on Cl^- binding in the dark was revealed experimentally.[28,29] The position of the Cl^- binding/interacting site in the CP channel at N is not clear at present. It is reasonable, however, to assume that the interaction with the OH group of Thr218 induces the prompt formation of N. Rate constant k_3 represents the process of uptake of Cl^- from the EC space, and the value is largest for the wild type. The fact that the wild-type k_3 value is the largest is not understood. Although the event occurs in the EC channel, Thr218 is located in the CP channel. Note that Thr218 is located close to the Schiff base.

Special Coordination of Water with the OH Group of Thr218 May Be Necessary. As shown in Table 1, the largest value of $K_{d,N\leftrightarrow O}$ is given by Thr (wild type), and although hydrophilicity or hydrophobicity may not be important, the OH group of Thr may be essential. As described above, we measured the partial molar volume change from N to O ($\Delta V_{N\rightarrow O}$) (see Table 1) from the pressure dependence of $K_{d,N\leftrightarrow O}$. Large volume changes of the proteins usually reflect changes in the hydration and packing states of the proteins. Volume increases were also observed in the M to N transition of the BR photocycle.[34,35] For BR, it has been widely considered that the outward tilting of helix F in the late M state allows water molecules to hydrate the CP channel and to create a transient hydrogen-bonded network.[43−46] The liquid water probably binds to the protein interior in a crystalline-like state, so the entry of water from the bulk phase could in part contribute to the volume increase. Similar to BR, water may enter NpHR at O (except for the V mutant), probably by the

dx.doi.org/10.1021/bi401295e | *Biochemistry* 2013, 52, 9257−9268

opening of helix F. In Figure 8, $K_{d,N\leftrightarrow O}$ values are plotted against $\Delta V_{N\to O}$. Both $K_{d,N\leftrightarrow O}$ and $\Delta V_{N\to O}$ are largest for the

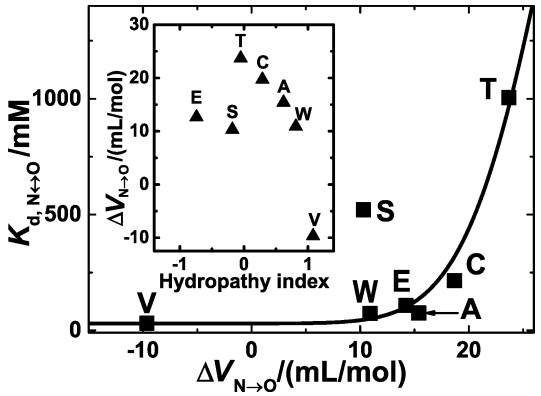

Figure 8. Plot of $K_{d,N\leftrightarrow O}$ values vs $\Delta V_{N\to O}$. In the inset, $\Delta V_{N\to O}$ is plotted vs the hydropathy index of the residue at position 218.

wild-type protein. Except for T218V, the amounts of water entered do not vary much for the mutants. This tendency is also seen in the inset of Figure 8, where $\Delta V_{N\to O}$ of various mutants is plotted against the hydropathy index. Thus, we infer that for the Cl^- release (the increase in $K_{d,N\leftrightarrow O}$), water entry is necessary but not sufficient. Special coordination between the entered water molecule and the OH group of Thr may be necessary. The X-ray structure showed the formation of a hydrogen bonding network among Thr218 (helix F), Ala255 (helix G), and Trp222 (helix F). The proper interaction of the OH group of Thr218 with the entered water disturbs the hydrogen bonding network, which induces the conformational changes of helices F and G and increases $K_{d,N\leftrightarrow O}$. These three residues are also conserved in BR as Thr178, Ala215, and Trp182, respectively. For BR, the photoinduced switches of the hydrogen bonding network are considered to cause the subsequent conformational changes in the CP channel.[46]

Cl^- Dependence of k_3. The concentration dependence of this rate constant is peculiar (see Figure 3). The curve is convex. This rate constant is for the O decay. Exactly this is the decay of P_3 (quasi-equilibrium between N and O). However, we assume that this decay is that of O in which the "external" Cl^- entered into the protein through the EC channel to the Cl^- binding site in the vicinity of retinal. Therefore, the rate should increase with an increase in Cl^- concentration. These values increase for the wild type and mutants until approximately the $K_{d,N\leftrightarrow O}$ value (Figure 3). k_3 should be expressed as

$$k_3 = k^0[O][Cl^-] \tag{7}$$

Here, k^0 is a constant. The O concentration, [O], is proportional to $K_{d,N\leftrightarrow O}/(K_{d,N\leftrightarrow O} + [Cl^-])$ (see eq S2 of the Supporting Information), and then

$$k_3 = k^0\frac{K_{d,N\leftrightarrow O}[Cl^-]}{K_{d,N\leftrightarrow O} + [Cl^-]} \tag{8}$$

k_3 is expected to exhibit Michaelis−Menten behavior. As shown in Figure 3, below the $K_{d,N\leftrightarrow O}$, eq 8 seems to hold. However, the values decrease at higher Cl^- concentrations. This might be explained if $[Cl^-]$ is not that of the external medium. There might also be a second Cl^- binding site. Mevorat-Kaplan et al.[47] suggested that in the dark state a chloride binding site on the EC channel with a dissociation constant of ~100 mM may be present. Recent X-ray crystal structure analysis also showed a weak Cl^- binding site on the EC side between the BC loop and FG loop.[48] During the O to NpHR′ transition, the Cl^- may move from this site to the binding site near the Schiff base. We assume that binding equilibrium of Cl^- between this binding site on the EC channel and the external medium is attained at O and that the transfer of Cl^- from this site to the vicinity of retinal is a rate-determining process. Under these assumptions, k_3 is expressed as follows instead of as in eq 8:

$$k_3 = k^0\frac{K_{d,N\leftrightarrow O}}{K_{d,N\leftrightarrow O} + [Cl^-]} \times \frac{[Cl^-]}{K_d' + [Cl^-]} \tag{9}$$

where K_d' is the dissociation constant of this second site at O. Thus, K_d' defines the equilibrium between two O intermediates: one O binds Cl^- at the second site, but another O does not. The mole fraction of the former O in this equilibrium is described by the last term of eq 9. Thus, eq 9 means that NpHR′ forms from O binding Cl^- at the second site. In the following considerations, we assume $K_d' < K_{d,N\leftrightarrow O}$. When $[Cl^-]$ is low, k_3 increases with the increase in $[Cl^-]$, reflecting the increase in the last term of eq 9. With a further increase in $[Cl^-]$, k_3 decreases because the middle term of eq 9 decreases while the last term is constant. During the subsequent NpHR′ to NpHR transition, uptake of Cl^- from the bulk to the second binding site could occur depending on $[Cl^-]$ and the dissociation constant of this site at the dark state. However, the rate constants (k_4) were independent of $[Cl^-]$ for all mutants and for the wild type; this rate inversely decreased with an increase in $[Cl^-]$ (Figure 3). Thus, there are other factors determining this rate. For the detailed molecular event, further studies are needed.

A mutant KM-1 of *N. pharaonis* was isolated by UV radiation. From this cell, a membrane fraction containing large amounts of NpHR can be isolated.[49] Using this membrane fraction, $K_{d,N\leftrightarrow O}$ was estimated to be ~4 M (data not shown). The value of $K_{d,N\leftrightarrow O}$ may be influenced by the presence of lipids, especially by tightly bound bacterioruberin or the solubilized state. For the KM-1 membrane, a decrease in k_3 was not observed at <4 M Cl^-, probably because of the large $K_{d,N\leftrightarrow O}$.

Effect of Mutations on Pumping Activity. The measurements of Cl^- pumping activities (results shown in Figures 5 and 6) are from the steady state experiments in which *E. coli* cells were illuminated by the constant light. On the other hand, other measurements are from the transient state experiments in which the NpHR samples were activated by the flash light. Photoinduced HR activity shown in Figures 5 and 6 may be primarily determined by the rate of cycling or the turnover rate.[8] Figure 3 shows that the slowest transition is k_4 (NpHR′ → NpHR). Therefore, the shift of the N ↔ O equilibrium and the change in k_2 and k_3 are not considered to affect the pumping activity. However, Figures 5 and 6A show the variation of the photoinduced proton uptake for the mutants. The uptake of intact cells was measured in the absence of CCCP, i.e., in the presence of membrane potential that was produced by intracellular metabolism. In addition, Figure 6C shows that the relative pumping activity increased with an increase in $K_{d,N\leftrightarrow O}$, indicating that the activity depends on the N ↔ O equilibrium. This means that when the equilibrium shifts to O, the pumping activity is increased. However, Figure 6B shows almost no variation or a smaller variation in mutant pumping activity. The cells used were de-energized cells prepared by being gently shaken for 2 h in the presence of

dx.doi.org/10.1021/bi401295e | *Biochemistry* 2013, 52, 9257−9268

CCCP; measurements were taken in the presence of CCCP, so no interior negative membrane potential was generated. An interior negative membrane potential hinders proton uptake because of the uphill transport, so the scale in Figure 6A is smaller than that in Figure 6B. Figure 3 shows that the slowest transitions of k_4 are almost equal to one another. The data in Figure 6B are understandable from the standpoint of the turnover rate. Of interest, for the de-energized cells, the mutants with immeasurably small $K_{d,N\leftrightarrow O}$ values (Gln, Met, Leu, Phe, and Ile) show a large response (Figure 6B), whereas those in the presence of membrane potential are small (Figure 6A). The difference between the energized and nonenergized cells is the presence or absence of interior negative membrane potential. Recently, we found that the interior negative membrane potential shifted the N ↔ O equilibrium to N, which decreases the O concentration and thereby decreases k_3 (see eq 7) (manuscript in preparation). Particularly for mutants with a small $K_{d,N\leftrightarrow O}$, the slowest process might become k_3 in the presence of membrane potential. The Cl^- release of these mutants might involve an electrogenicity larger than that of the wild type. In the presence of membrane potential, this larger electrogenicity might contribute to the substantial delay of k_3 through the remarkable shift of the N ↔ O equilibrium toward N. These mutants have low activity in the presence of membrane potential. In other words, a high concentration of O is necessary not to decrease the activity in the presence of membrane potential, and in this sense, Thr at position 218 is suitable. Another possibility is that when the N ↔ O equilibrium shifts greatly to N, most NpHR returns to the original state through a nonelectrogenic pathway (such as N → NpHR′ or NpHR). Hackmann et al.[36] previously proposed a similar nonelectrogenic pathway based on time-resolved FTIR measurements at a high concentration of Cl^-, although they proposed an L_2 → NpHR pathway.

Comparison of HsHR with NpHR. Váró et al. described the photocycle of HsHR as HsHR → K ↔ L_1 ↔ L_2 ↔ N → HsHR and found that the rate constants did not show any Cl^- dependence or very weak Cl^- dependence.[9] Comparison with the NpHR cycle indicates that the HsHR cycle lacks the O intermediate, but they considered that the missing of O may have a kinetic cause. The missing O may eliminate the Cl^--dependent process. On the basis of our analysis, we infer that the $K_{d,N\leftrightarrow O}$ of the N ↔ O quasi-equilibrium largely shifts to N for HsHR. The residue at position 218 is not the only factor determining $K_{d,N\leftrightarrow O}$ because the corresponding residue of HsHR is Thr203. There are other factor(s) determining $K_{d,N\leftrightarrow O}$.

CONCLUSIONS

We made various NpHR Thr218 mutants and examined their photochemistry. The photochemically defined intermediate P_3 consists of a quasi-equilibrium between the N and O intermediates. The equilibrium constant $K_{d,N\leftrightarrow O}$ was defined in eq 3, and $K_{d,N\leftrightarrow O}$ was largest for wild-type NpHR. The partial molar volume changes between N and O states ($\Delta V_{N\rightarrow O}$) were estimated from the pressure dependence of $K_{d,N\leftrightarrow O}$. Except for T218V, the volume of O is larger than that of N. If the volume change of the protein is due to the change in hydration, water could enter through the F helix opening, which occurs in BR. The largest $K_{d,N\leftrightarrow O}$ and $\Delta V_{N\rightarrow O}$ values were obtained from the wild type, whereas for some mutants, $\Delta V_{N\rightarrow O}$ was large but $K_{d,N\leftrightarrow O}$ was small. These findings may indicate that water entry is necessary but not sufficient. Special coordination of the water molecule with the OH group of the Thr at position 218 may be necessary to release Cl^- into the CP space. Rate constants k_2 and k_3 are largest for the wild type. The wild-type protein rapidly transfers Cl^- from the binding site near the Schiff base in the dark to the CP space. k_3 showed a convex curve with respect to the Cl^- concentration, leading to the hypothesis that a second Cl^- binding site exists in the EC channel (see eq 9). This should be investigated further. The pumping activity in the presence of interior negative membrane potential increased with an increase in $K_{d,N\leftrightarrow O}$. However, for de-energized cells in the presence of CCCP, activities were almost the same for all mutants. Although one possible reason was described above, further investigation is required to determine the true cause. However, the measurements in the presence of CCCP might not be the true activity in some cases.

ASSOCIATED CONTENT

Supporting Information

Determination of the absolute spectra of P_i intermediates (Figure S1), calculation of $K_{d,N\leftrightarrow O}$ values of the wild type and mutants (Figure S2), pressure dependences of P_i spectra (Figure S3), and activation volumes associated with the decay of P_i intermediates (Figure S4). This material is available free of charge via the Internet at http://pubs.acs.org.

AUTHOR INFORMATION

Corresponding Author

*Telephone and fax: +81-11-706-2771. E-mail: demura@sci.hokudai.ac.jp.

Author Contributions

K.S. and H.S. contributed equally to this work.

Funding

This work was supported by grants from the Japanese Ministry of Education, Culture, Sports, Science, and Technology to T.K. (23510251) and M.D. (23657096).

Notes

The authors declare no competing financial interest.

ABBREVIATIONS

HR, halorhodopsin; NpHR, HR from *N. pharaonis*; HsHR, HR from *H. salinarum*; CP, cytoplasmic; EC, extracellular; FTIR, Fourier transform infrared; $K_{d,N\leftrightarrow O}$, dissociation constant defined in eq 3; K_d', dissociation constant of the assumed Cl^- binding site at the end of EC channel at O; $\Delta V_{N\rightarrow O}$, partial molar volume change between N and O with reference to N (see eq 6); SG, skewed Gaussian; f, fraction of N of N−O equilibrium; P_i, ith photochemically defined intermediate (i = 1−4); k_i, decay kinetic constant of P_i; CCCP, carbonyl cyanide *m*-chlorophenylhydrazone.

REFERENCES

(1) Matsuno-Yagi, A., and Mukohata, Y. (1980) ATP synthesis linked to light-dependent proton uptake in a red mutant strain of *Halobacterium* lacking bacteriorhodopsin. *Arch. Biochem. Biophys. 199*, 297−303.

(2) Schobert, B., and Lanyi, J. K. (1982) Halorhodopsin is a light-driven chloride pump. *J. Biol. Chem. 257*, 10306−10313.

(3) Bamberg, E., Hegemann, P., and Oesterhelt, D. (1984) The chromoprotein of halorhodopsin is the light-driven electrogenic chloride pump in *Halobacterium halobium*. *Biochemistry 23*, 6216−6221.

(4) Lanyi, J. K. (1990) Halorhodopsin, a light-driven electrogenic chloride-transport system. *Physiol. Rev. 70*, 319−330.

(5) Váró, G. (2000) Analogies between halorhodopsin and bacteriorhodopsin. *Biochim. Biophys. Acta 1460*, 220−229.
(6) Gerscher, S., Mylrajan, M., Hildebrandt, P., Baron, M.-H., Müller, R., and Engelhard, M. (1997) Chromophore-anion interactions in halorhodopsin from *Natronobacterium pharaonis* probed by time-resolved resonance Raman spectroscopy. *Biochemistry 36*, 11012−11020.
(7) Váró, G., Brown, L. S., Sasaki, J., Kandori, H., Maeda, A., Needleman, R., and Lanyi, J. K. (1995) Light-driven chloride ion transport by halorhodopsin from *Natronobacterium pharaonis*. I. The photochemical cycle. *Biochemistry 34*, 14490−14499.
(8) Kamo, N., Takeuchi, M., Hazemoto, N., and Kobatake, Y. (1983) Light-induced ΔpH of envelope vesicles containing halorhodopsin measured by use of a spin probe. *Arch. Biochem. Biophys. 221*, 514−525.
(9) Váró, G., Zimányi, L., Fan, X., Sun, L., Needleman, R., and Lanyi, J. K. (1995) Photocycle of halorhodopsin from *Halobacterium salinarium*. *Biophys. J. 68*, 2062−2072.
(10) Zimányi, L., and Lanyi, J. K. (1997) Fourier transform Raman study of retinal isomeric composition and equilibration in halorhodopsin. *J. Phys. Chem. B 101*, 1930−1933.
(11) Hohenfeld, I. P., Wegener, A. A., and Engelhard, M. (1999) Purification of histidine tagged bacteriorhodopsin, *pharaonis* halorhodopsin and *pharaonis* sensory rhodopsin II functionally expressed in *Escherichia coli*. *FEBS Lett. 442*, 198−202.
(12) Sato, M., Kanamori, T., Kamo, N., Demura, M., and Nitta, K. (2002) Stopped-flow analysis on anion binding to blue-form halorhodopsin from *Natronobacterium pharaonis*: Comparison with the anion-uptake process during the photocycle. *Biochemistry 41*, 2452−2458.
(13) Yamashita, Y., Kikukawa, T., Tsukamoto, T., Kamiya, M., Aizawa, T., Kawano, K., Miyauchi, S., Kamo, N., and Demura, M. (2011) Expression of *salinarum* halorhodopsin in *Escherichia coli* cells: Solubilization in the presence of retinal yields the natural state. *Biochim. Biophys. Acta 1808*, 2905−2912.
(14) Ludmann, K., Ibron, G., Lanyi, J. K., and Váró, G. (2000) Charge motions during the photocycle of *pharaonis* halorhodopsin. *Biophys. J. 78*, 959−966.
(15) Essen, L.-O. (2002) Halorhodopsin: Light-driven ion pumping made simple? *Curr. Opin. Struct. Biol. 12*, 516−522.
(16) Chizhov, I., and Engelhard, M. (2001) Temperature and halide dependence of the photocycle of halorhodopsin from *Natronobacterium pharaonis*. *Biophys. J. 81*, 1600−1612.
(17) Hasegawa, C., Kikukawa, T., Miyauchi, S., Seki, A., Sudo, Y., Kubo, M., Demura, M., and Kamo, N. (2007) Interaction of the halobacterial transducer to a halorhodopsin mutant engineered so as to bind the transducer: Cl^- circulation within the extracellular channel. *Photochem. Photobiol. 83*, 293−302.
(18) Chizhov, I., Chernavskii, D. S., Engelhard, M., Mueller, K. H., Zubov, B. V., and Hess, B. (1996) Spectrally silent transitions in the bacteriorhodopsin photocycle. *Biophys. J. 71*, 2329−2345.
(19) Oesterhelt, D. (1995) Structure and function of halorhodopsin. *Isr. J. Chem. 35*, 475−494.
(20) Chon, Y.-S., Kandori, H., Sasaki, J., Lanyi, J. K., Needleman, R., and Maeda, A. (1999) Existence of two L photointermediates of halorhodopsin from *Halobacterium salinarum*, differing in their protein and water FTIR bands. *Biochemistry 38*, 9449−9455.
(21) Váró, G., Needleman, R., and Lanyi, J. K. (1995) Light-driven chloride ion transport by halorhodopsin from *Natronobacterium pharaonis*. II. Chloride release and uptake, protein conformation change, and thermodynamics. *Biochemistry 34*, 14500−14507.
(22) Inoue, K., Kubo, M., Demura, M., Kamo, N., and Terazima, M. (2009) Reaction dynamics of halorhodopsin studied by time-resolved diffusion. *Biophys. J. 96*, 3724−3734.
(23) Lanyi, J. K., and Vodyanoy, V. (1986) Flash spectroscopic studies of the kinetics of the halorhodopsin photocycle. *Biochemistry 25*, 1465−1470.
(24) Ames, J. B., Raap, J., Lugtenburg, J., and Mathies, R. A. (1992) Resonance Raman study of halorhodopsin photocycle kinetics, chromophore structure, and chloride-pumping mechanism. *Biochemistry 31*, 12546−12554.
(25) Guijarro, J., Engelhard, M., and Siebert, F. (2006) Anion uptake in halorhodopsin from *Natromonas pharaonis* studied by FTIR spectroscopy: Consequences for the anion transport mechanism. *Biochemistry 45*, 11578−11588.
(26) Rüdiger, M., Haupts, U., Gerwert, K., and Oesterhelt, D. (1995) Chemical reconstitution of a chloride pump inactivated by a single point mutation. *EMBO J. 14*, 1599−1606.
(27) Rüdiger, M., and Oesterhelt, D. (1997) Specific arginine and threonine residues control anion binding and transport in the light-driven chloride pump halorhodopsin. *EMBO J. 16*, 3813−3821.
(28) Sato, M., Kikukawa, T., Araiso, T., Okita, H., Shimono, K., Kamo, N., Demura, M., and Nitta, K. (2003) Roles of Ser130 and Thr126 in chloride binding and photocycle of *pharaonis* halorhodopsin. *J. Biochem. 134*, 151−158.
(29) Sato, M., Kikukawa, T., Araiso, T., Okita, H., Shimono, K., Kamo, N., Demura, M., and Nitta, K. (2003) Ser-130 of *Natronobacterium pharaonis* halorhodopsin is important for the chloride binding. *Biophys. Chem. 104*, 209−216.
(30) Sato, M., Kubo, M., Aizawa, T., Kamo, N., Kikukawa, T., Nitta, K., and Demura, M. (2005) Role of putative anion-binding sites in cytoplasmic and extracellular channels of *Natronomonas pharaonis* halorhodopsin. *Biochemistry 44*, 4775−4784.
(31) Seki, A., Miyauchi, S., Hayashi, S., Kikukawa, T., Kubo, M., Demura, M., Ganapathy, V., and Kamo, N. (2007) Heterologous expression of *pharaonis* halorhodopsin in *Xenopus laevis* oocytes and electrophysiological characterization of its light-driven Cl^- pump activity. *Biophys. J. 92*, 2559−2569.
(32) Kubo, M., Kikukawa, T., Miyauchi, S., Seki, A., Kamiya, M., Aizawa, T., Kawano, K., Kamo, N., and Demura, M. (2009) Role of Arg123 in light-driven anion pump mechanisms of *pharaonis* halorhodopsin. *Photochem. Photobiol. 85*, 547−555.
(33) Kolbe, M., Besir, H., Essen, L. O., and Oesterhelt, D. (2000) Structure of the light-driven chloride pump halorhodopsin at 1.8 Å resolution. *Science 288*, 1390−1396.
(34) Váró, G., and Lanyi, J. K. (1995) Effects of hydrostatic pressure on the kinetics reveal a volume increase during the bacteriorhodopsin photocycle. *Biochemistry 34*, 12161−12169.
(35) Kikukawa, T., Saha, C. K., Balashov, S. P., Imasheva, E. S., Zaslavsky, D., Gennis, R. B., Abe, T., and Kamo, N. (2008) The lifetimes of *pharaonis phoborhodopsin* signaling states depend on the rates of proton transfers: Effects of hydrostatic pressure and stopped flow experiments. *Photochem. Photobiol. 84*, 880−888.
(36) Hackmann, C., Guijarro, J., Chizhov, I., Engelhard, M., Rödig, C., and Siebert, F. (2001) Static and time-resolved step-scan fourier transform infrared investigations of the photoreaction of halorhodopsin from *Natronobacterium Pharaonis*: Consequences for models of the anion translocation mechanism. *Biophys. J. 81*, 394−406.
(37) Shibata, M., Saito, Y., Demura, M., and Kandori, H. (2006) Deprotonation of Glu234 during the photocycle of *Natronomonas pharaonis* halorhodopsin. *Chem. Phys. Lett. 432*, 545−547.
(38) Bogomolni, R. A., Stoeckenius, W., Szundi, I., Perozo, E., Olson, K. D., and Spudich, J. L. (1994) Removal of transducer HtrI allows electrogenic proton translocation by sensory rhodopsin I. *Proc. Natl. Acad. Sci. U.S.A. 91*, 10188−10192.
(39) Sudo, Y., Iwamoto, M., Shimono, K., Sumi, M., and Kamo, N. (2001) Photo-induced proton transport of *pharaonis* phoborhodopsin (sensory rhodopsin II) is ceased by association with the transducer. *Biophys. J. 80*, 916−922.
(40) Muneyuki, E., Shibazaki, C., Ohtani, H., Okuno, D., Asaumi, M., and Mogi, T. (1999) Time-resolved measurements of photovoltage generation by bacteriorhodopsin and halorhodopsin adsorbed on a thin polymer film. *J. Biochem. 125*, 270−276.
(41) Gmelin, W., Zeth, K., Efremov, R., Heberle, J., Tittor, J., and Oesterhelt, D. (2007) The crystal structure of the L1 intermediate of halorhodopsin at 1.9 Å resolution. *Photochem. Photobiol. 83*, 369−377.
(42) Kouyama, T., Kanada, S., Takeguchi, Y., Narusawa, A., Murakami, M., and Ihara, K. (2010) Crystal structure of the light-

driven chloride pump halorhodopsin from *Natronomonas pharaonis*. *J. Mol. Biol. 396*, 564−579.
(43) Sass, H. J., Buldt, G., Gessenich, R., Hehn, D., Neff, D., Schlesinger, R., Berendzen, J., and Ormos, P. (2000) Structural alterations for proton translocation in the M state of wild-type bacteriorhodopsin. *Nature 406*, 649−653.
(44) Maeda, A., Gennis, R. B., Balashov, S. P., and Ebrey, T. G. (2005) Relocation of water molecules between the Schiff base and the Thr46-Asp96 region during light-driven unidirectional proton transport by bacteriorhodopsin: An FTIR study of the N intermediate. *Biochemistry 44*, 5960−5968.
(45) Schobert, B., Brown, L. S., and Lanyi, J. K. (2003) Crystallographic structures of the M and N intermediates of bacteriorhodopsin: Assembly of a hydrogen-bonded chain of water molecules between Asp-96 and the retinal Schiff base. *J. Mol. Biol. 330*, 553−570.
(46) Lanyi, J. K. (2004) Bacteriorhodopsin. *Annu. Rev. Physiol. 66*, 665−688.
(47) Mevorat-Kaplan, K., Brumfeld, V., Engelhard, M., and Sheves, M. (2006) The protonated Schiff base of halorhodopsin from *Natronobacterium pharaonis* is hydrolyzed at elevated temperatures. *Photochem. Photobiol. 82*, 1414−1421.
(48) Kanada, S., Takeguchi, Y., Murakami, M., Ihara, K., and Kouyama, T. (2011) Crystal structures of an O-like blue form and an anion-free yellow form of *pharaonis* halorhodopsin. *J. Mol. Biol. 413*, 162−176.
(49) Ihara, K., Narusawa, A., Maruyama, K., Takeguchi, M., and Kouyama, T. (2008) A halorhodopsin-overproducing mutant isolated from an extremely haloalkaliphilic archaeon *Natronomonas pharaonis*. *FEBS Lett. 582*, 2931−2936.
(50) Eisenberg, D., Weiss, R. M., Terwilliger, T. C., and Wilcox, W. (1982) Hydrophobic moments and protein structure. *Faraday Symp. Chem. Soc. 17*, 109−120.